Chemical Physics Letters 771 (2021) 138522

Contents lists available at ScienceDirect

Chemical Physics Letters

journal homepage: www.elsevier.com/locate/cplett

Research paper

Halogen bond interaction: Role of hybridization and induction

Francesca Nunzi [a,b,*], Diego Cesario [a], Francesco Tarantelli [a,b], Leonardo Belpassi [b]

[a] Dipartimento di Chimica, Biologia e Biotecnologie, via Elce di Sotto 8, I-06123 Perugia, Italy
[b] Istituto CNR di Scienze e Tecnologie Chimiche "Giulio Natta" (CNR-SCITEC), via Elce di Sotto, I-06123 Perugia, Italy

ARTICLE INFO

Keywords:
Density functional
Charge displacement
Force-fields
Polar flattening - σ-hole
Charge transfer

ABSTRACT

Selected systems bearing carbon-chlorine (C—Cl) bond and their complexes with two representative Lewis bases have been examined by means of quantum-chemistry DFT calculations to gain a deeper insight into the parameters affecting the halogen bond (XB) interaction. The dependence of the C hybridization (sp, sp^2, sp^3) and induction (by replacing the H atoms with the F electron-withdrawing atoms) on the polar flattening (PF), the σ-hole and the charge transfer (CT) in the XB complex has been unraveled.

1. Introduction

The halogen bond (XB) has recently gained increasing interest in the field of non-covalent interactions, next to the ubiquitous hydrogen bond. Several peculiar features of XB, such as the high directionality and strength tunability, prompted a plethora of applications in organocatalysis, crystal engineering and drug design. Based on the definition of International Union of Pure and Applied Chemistry (IUPAC) [1], XB is a non-covalent weak interaction occurring "between an electrophilic region, associated with a halogen (X) atom in a molecular entity, and a nucleophilic region in another, or the same, molecular entity''. Even if the forces involved in XB are primarily electrostatic in nature, other components, such as repulsion, dispersion, induction or charge transfer (CT), may concur to the definition of the XB strength [2–10]. The electrostatic origin of the XB interaction relies on the σ-hole concept, pointing at a positive electrostatic potential surface (ESP) on the X atom towards an incoming negative electron donor [11–14]. In addition, the short intermolecular distances occurring in XB adducts may be also related to the peculiar X electron density, being not spherically symmetric, as in the isolated atom, but flattened along the X covalent bond direction [11,15]. This so-called electron density "polar flattening" (PF) is expected to reduce the short-range repulsion energy contribution in the interaction of the halogenated substrate with a partner approaching along the outer side of the X covalent bond [4,6,16]. Depending on the nature of the halogenated substrate and/or of the interacting partner, a transfer of electron density can actually occur upon XB formation, thus pointing at a covalent contribution to the overall bonding energy, namely the CT component [2,17–19]. Assuming $(ns^2)(np_x^2)(np_y^2)(np_z^1)$ as X valence electron configuration, with the z axis taken along the X covalent bond, the unpaired electron in the p_z orbital results mostly localized in the X covalent bond region, leaving a lack of electron density in the outer lobe, that is related to both PF and σ-hole features. Conversely, the electron pairs in the p_x/p_y orbitals perpendicular to the bond axis produce an electron negative region around the X atom (electron density polar elongation, PE), suitable for electron-deficient partner attacks.

In this work we focus on the C-Cl bond as prototype for the C-X covalent bond in halogenated substrates and we examined by means of quantum-chemistry calculations (DFT) ten reference chlorinated hydrocarbon substrates, differing for the carbon hybridization degree and/or chemical environment. Specifically, we considered chloromethane (CH_3Cl, **1**), chloroethylene (CH_2CHCl, **2**), and chloroethyne (CHCCl, **3**), containing, respectively, a sp^3, sp^2 and sp C atom bonded to the chlorine centre (see Fig. 1). For the sake of comparison, we also considered systems where the Cl atom is bonded to an aromatic sp^2 (chlorobenzene, C_6H_5Cl, **4**) and to a C atom in imidazole cation ($[C_3N_2H_4Cl]^+$, **5**). By replacing the hydrogen with fluorine atoms, we gained the correspondent fluorinated substrates, labelled as **1F** – **5F**. In addition, we selected a negative charged (Cl^-) and neutral (NH_3) Lewis bases, as interacting partners assisting the XB adduct formation with the above cited hydrocarbon substrates. We analyzed how the hybridization and fluorine substitution affect the PF, the σ-hole and the electron charge amount transferred upon XB complex formation. Charge displacement (CD) analysis is applied to quantitatively evaluate the CT [20]. The information derived from our approach can be very helpful in the optimization of adequate force-fields for the modeling of the HX interaction,

* Corresponding author at: Dipartimento di Chimica, Biologia e Biotecnologie, via Elce di Sotto 8, I-06123 Perugia, Italy.
E-mail address: francesca.nunzi@unipg.it (F. Nunzi).

https://doi.org/10.1016/j.cplett.2021.138522
Received 13 January 2021; Accepted 5 March 2021
Available online 17 March 2021

for which it is of fundamental importance a comprehensive understanding of how much PF, σ-hole and CT behave as local features, that means that they are independent from the specific chemical environment, or, rather, they are transferable among various different substrates.

2. Methodology

2.1. Computational Settings

Molecular geometry optimizations on the selected halogenated molecules and their complexes with Cl^- and NH_3 partners are carried out without symmetry constraints at the density functional level of theory, employing the gradient corrected BP86 functional [21,22], by using the Gaussian 09 code [23]. The standard Dunning's correlation consistent basis set aug-cc-pVTZ (AVTZ) is used for the C, H, N, F, and Cl atoms (see Tables S1-S3 in the Supplementary Data section) [24]. For the sake of comparison, for the selected system **1** CH_3Cl, geometry optimizations have been also performed with the hybrid B3LYP/BPE0 [25–27] and long-range corrected CAM-B3LYP [28] functionals and with *ab initio* calculations at the coupled-cluster level of theory [29], with single, double and perturbatively included triple excitations, CCSD (T), with AVTZ basis set, by means of the MOLPRO program [30]. The results are reported in Table S2 in the Supplementary Data section and show only minor deviations (within 0.02 Å and 0.2° for the bond distances and angles, respectively).

2.2. Polar flattening (PF) and equatorial elongation (EE)

To quantitatively evaluate the chlorine electron density PF, we compare the electron density profiles along the C—Cl bond axis (z, in the present reference) with that of a spherical isolated Cl atom, placed at the same position of Cl in the halogenated molecules. A measure of the density shift may be provided by the Δz value, defined as the difference on the C—Cl bond axis between the projection of two isodensity points [one for the spherical isolated Cl atom and the other in the halogenated molecule, $\Delta z = z_{Cl(isolated)} - z_{Cl(system)}$]. The specific isodensity value is clearly arbitrary, however may be chosen to distinctively estimate the Δz PF of the X electron density (hereafter labelled as Δz_{PF}). A common selection is the proposal from Bader *et al.* for an isodensity value of 0.001 e·bohr^{-3} [31], referred to a molecular surface encompassing approximately 96% of the overall electronic charge of a molecule. In the following we will refer to this advice for consistency.

Comparing the density profile of the halogen atom along the directions perpendicular to the C—Cl bond axis (x, y) with the spherical density profile of the isolated Cl atom, a deformation (equatorial

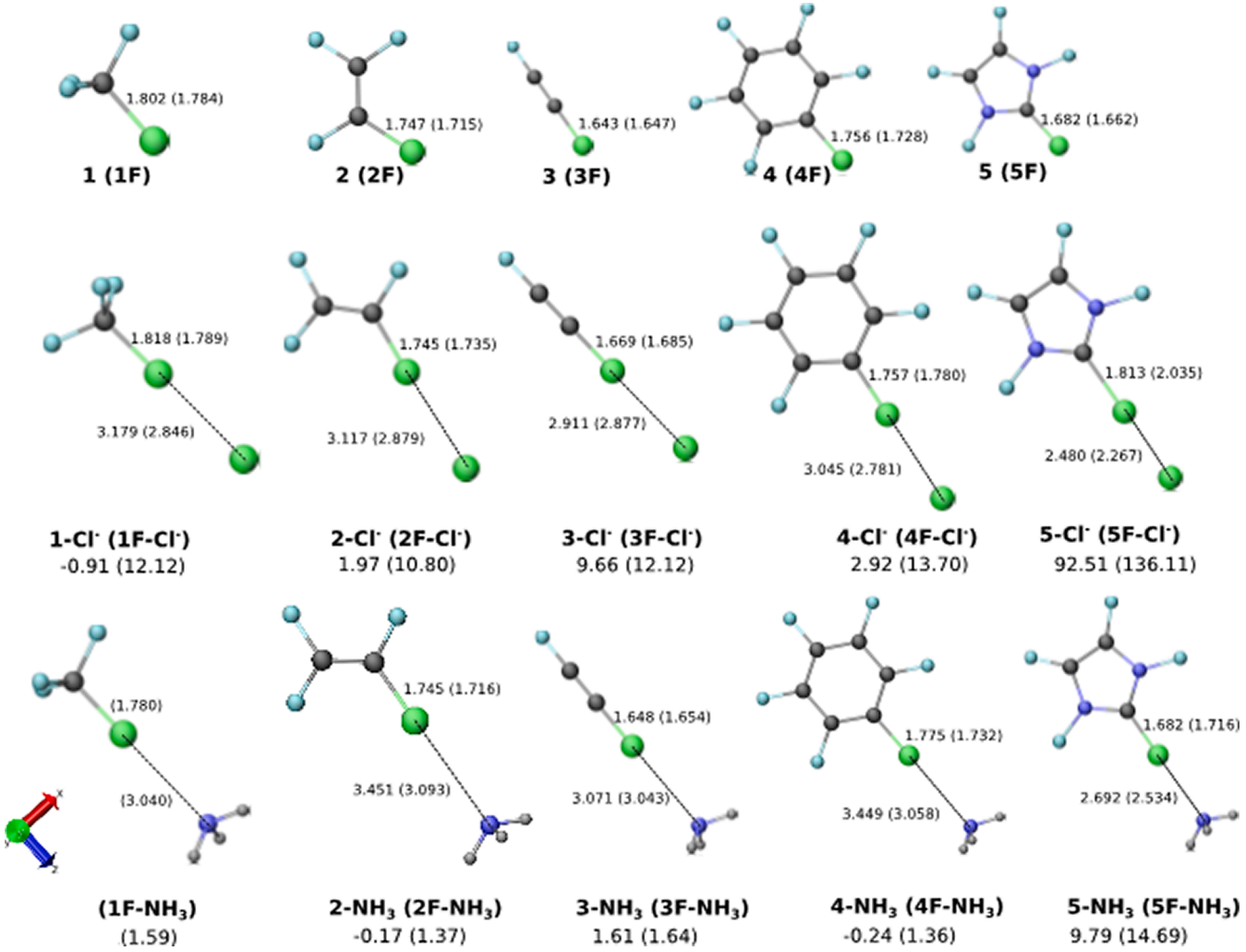

Fig. 1. Structures of investigated hydrocarbons (top), namely CH_3Cl, **1** (CF_3Cl, **1F**), CH_2CHCl, **2** (CF_2CFCl, **2F**), CHCCl, **3** (CFCCl, **3F**), C_6H_5Cl, **4** (C_6F_5Cl, **4F**) and $[C_3N_2H_4Cl]^+$, **5** ($[C_3N_2F_4Cl]^+$, **5F**) and of their complexes with Cl^- (middle) and NH_3 (bottom) Lewis bases. Selected bond distances in angstrom and interaction energies in kcal/mol are also reported (the values in parenthesis refer to the fluorinated systems **1F-5F**). C, gray; Cl, green; N, violet; F or H on hydrocarbons, light blue; H, light gray. The reference axes are also shown.

elongation, EE) of the bonded halogen atom electron density is analogously measured by $\Delta x = x_{Cl(isolated)}\text{-}x_{Cl(system)}$ and $\Delta y = y_{Cl(isolated)}\text{-}y_{Cl(system)}$ values. Δx and Δy values at the isodensity reference value of 0.001 e·bohr^{-3} are hereafter labelled as Δx_{EE} and Δy_{EE}.

We note that, limited to molecules with cylindrical symmetry, the PF can be evaluated as the difference between the distances, at a specific isodensity value, from the atom nucleus in the direction perpendicular and parallel to the C-Cl covalent bond [15]. Remarkably, for the investigated systems with π conjugation, we found markedly different values for Δx_{EE} and Δy_{EE} values (see below).

2.3. σ-hole

For a set of atomic nuclei and electrons, the electrostatic potential V at spatial position $\boldsymbol{r}$ is:

$$V(\boldsymbol{r}) = \sum_A \frac{Z_A}{|\boldsymbol{r}_A - \boldsymbol{r}|} - \int \frac{\rho(\boldsymbol{r}_e)}{|\boldsymbol{r}_e - \boldsymbol{r}|} d\boldsymbol{r}_e \quad (1)$$

where Z_A is the charge of nucleus A located at position $\boldsymbol{r}_A$ and $\rho(\boldsymbol{r}_e)$ is the electron density at position $\boldsymbol{r}_e$. The first positive term accounts for the positive Coulomb potential generated by the atomic nuclei, while the latter negative term refers to the electron cloud. Here we focus on the ESP along the C—X bond direction, being the XB axis, since it can be related to the electrostatic part of the XB interaction. The σ-hole magnitude is evaluated as the maximum positive value of ESP on top of the X atom, opposite to C, at the isodensity surface of 0.001 e·Bohr^{-3} [31].

2.4. Charge Transfer (CT)

The CT component is evaluated with the CD function [20], defined as:

$$Q(z) = \int_{-\infty}^{+\infty} dx \int_{-\infty}^{+\infty} dy \int_{-\infty}^{z} \Delta\rho(x, y, z')dz' \quad (2)$$

where the z axis joins the two atoms and $\Delta\rho$ is the electron density difference between the complex and the isolated noninteracting fragments (chlorinated hydrocarbon substrate and Lewis base), placed at the same positions they occupy in the complex. $Q(z)$ measures the electron charge that, upon formation of the adduct, is displaced, toward decreasing z values, across a plane through z perpendicular to the axis. A positive (negative) value corresponds to electrons flowing in the direction of decreasing (increasing) z. Accordingly, if the CD curve results appreciably different from zero and does not change in sign in the region between the fragments, we can unambiguously assert that a CT has occurred. Conversely, if the curve crosses zero in this region, the CT may be uncertain (both in magnitude and direction). If CT really takes place, it is useful, for comparative purpose, to end up with a definite numerical estimation of it, by considering the CD function value at a specific point between the fragments along the z axis. We selected the point along z where the non-interacting fragments electron densities become equal (that is the isodensity boundary, IB). This choice is reasonable, especially for small weakly interacting systems. Remarkably, the CD function represents a versatile tool for the assessment of the whole electron cloud rearrangement arising from all interaction components, unhampered by any specific decomposition scheme and it has been successfully employed also in the characterization of weakly-bound systems [4–8,32–34].

3. Results and discussion

3.1. Polar flattening (PF)

In Fig. 2 we compare the Cl electron density profile along the C-Cl bond for the selected system **2** with that for a spherical isolated Cl atom.

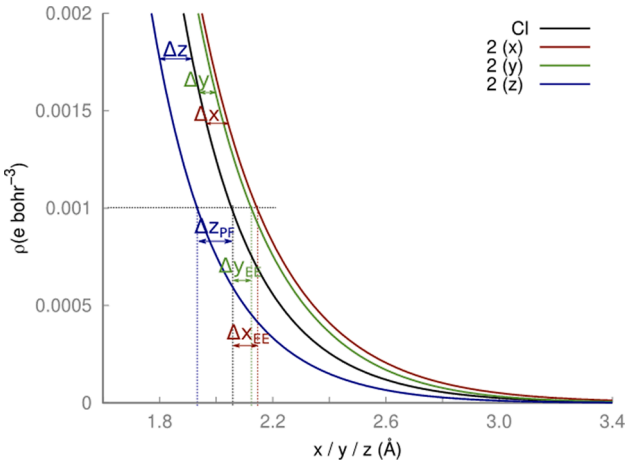

Fig. 2. Electron density profiles, ρ (e Bohr^{-3}), at the chlorine atom in the halogenated molecule, **2**, compared to that of the atomic Cl placed in the same position of Cl in the halogenated molecule. The z axis is in the direction along the C-Cl bond. The origin of the Cartesian coordinate system coincides with the Cl nuclei position. The Δx/Δy/Δz values are also shown (see text for details).

The flattening of the halogen clearly emerges, being the density profile systematically lower than that of the isolated atom. On the optimized **1**–**5**/**1F**-**5F** structures, we computed the electron density profiles of the Cl atom along the C—Cl bond axis, that is z, in the present molecular orientation (see Fig. 3a). Moving from sp^3 to sp^2 and sp carbon hybridization, the electron density profiles result more flattened, both in

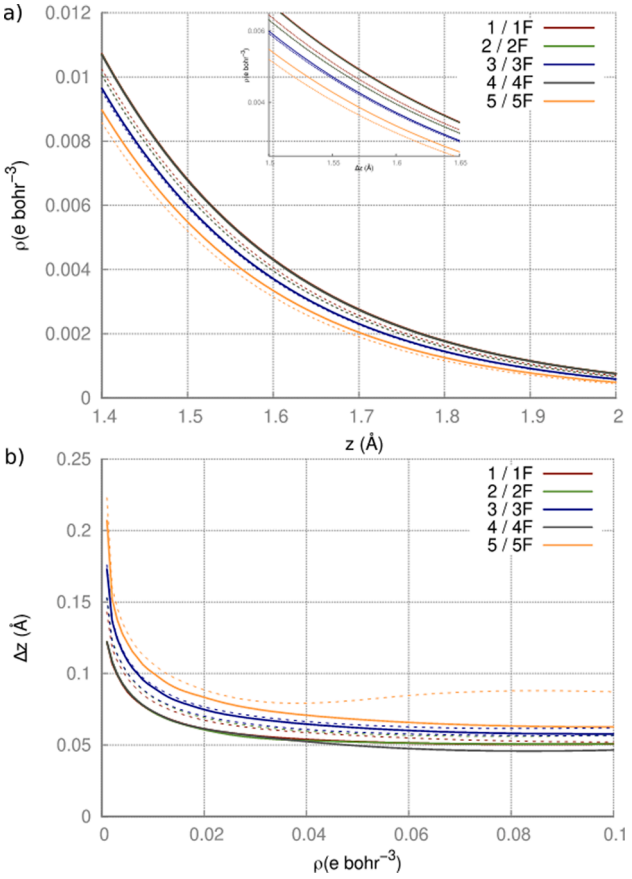

Fig. 3. a) Electron density profile, ρ (e Bohr^{-3}), along the C—Cl bond axis, z (Å), for the Cl atom in the halogenated molecules **1**–**5** and **1F**-**5F**; b) dependence of the polar flattening Δz (Å) on the isodensity surface ρ (e·Bohr^{-3}). Solid/dashed lines refer to hydrogenated/fluorinated systems.

hydrogenated and fluorinated molecules sets. **2** and **4**/**2F** and **4F** have the same density profile, suggesting that the aromaticity phenyl ring is irrelevant for the electron density at the Cl site. Remarkably, **5**/**5F** systems, having carbon hybridization similar to **2**/**2F** and **4**/**4F**, show the most flattened electron density profiles, that can be related with the molecule positive charge on the imidazole cation and with the shorter C-Cl bond distance (1.682/1.662 Å in **5**/**5F** vs 1.747/1.715 and 1.756/1.728 Å, respectively for **2**/**2F**, **4**/**4F**, see Fig. 1). By replacing hydrogen with fluorine atoms (**1**–**5** vs **1F**-**5F** systems), a mild flattening of the electron density profiles is attained, except for **3** vs **3F** system, showing almost coincident profiles This is not surprisingly in that the fluorine atom (due to the triple C-C bond) cannot be directly bonded to the halogenated carbon atom.

According to the PF definition (see above), we report in Fig. 3b the dependence of the Δz value on the electron density ρ for both the hydrogenated and fluorinated systems. Considering suitable values along the density profiles, the PF, estimated as Δz, assumes a narrow range of values (0.05–0.22 Å).

Our analysis shows that the PF value decreases in the order **5** > **3** > **4** ≈ **2** ≈ **1**. This trend can be explained on the basis of the carbon electronegativity: changing hybridization from sp^3 to sp, the s-character percentage increases, so that the carbon nucleus is less shielded, and the carbon atom results more electronegative. Consequently, the X electron cloud is more easily deformed when X is bonded to a sp with respect to sp^2 or sp^3 C atom. The most contracted electron densities in **5** can be related to the positive charge on the imidazole residue.

The **1F** – **5F** systems show slightly higher Δz values with respect to the correspondent **1** – **5** ones, since the substitution of hydrogen with electron withdrawing fluorine atoms makes the halogenated moiety more electronegative, so that the X density is still more easily distorted. The **3**/**3F** systems deviate from this rule of thumb, because of the absence of fluorine atoms directly bonded to the halogenated carbon atom. The fluorination keeps almost unaltered the pattern of the hybridization effect, with PF values decreasing in the order **5F** > **3F** > **4F** ≈ **2F** ≈ **1F**, as already shown for the hydrogenated systems.

Fig. 3b also shows that the Δz values increase with the decreasing of the isodensity values, ranging from about 0.05 to 0.22 Å. For isodensity values larger than 0.04 e·bohr^{-3} the Δz values remain very stable.

The Δz_{PF} values, evaluated at the reference isodensity value of 0.001 e·bohr^{-3} (see Table 1), increase from 0.12 Å in **1**, **2**, **4** systems up to a maximum of 0.22 Å in **5F**. On overall, the variations of the Δz_{PF} values upon hybridization or fluorine substitution are in agreement with the Δz trend discussed above, with percentage variations, computed as $\Delta z_{PF}/z_{Cl\ (isolated)}$*100, in the range 6–11%.

It is now interesting to investigate the electron density distortion occurring at X in the directions perpendicular to the XB. For the selected system **2**, the electron densities of the bonded chlorine along the *x* and *y* directions are found to be systematically higher than that of the isolated Cl atom (see Fig. 2), thus suggesting that the electron density anisotropy in bonded chlorine involves the whole X density and not only the density along the C—Cl bond direction.

Table 1 shows that in **1** the $-\Delta x_{PE}$ and $-\Delta y_{PE}$ have fairly the same values (0.09 Å), since the filled p_x/p_y chlorine orbitals are not involved in the C—Cl bond. **2** and **4** systems show different $-\Delta y_{PE}$ and $-\Delta x_{PE}$ values, $-\Delta x_{PE}$ being always higher (5.6 vs 3.1% in **2** and 8.1 vs 2.3% in **4**): being *xz* the molecule plane, the Cl p_y orbital is constrained in the C—C conjugation, thus being less prone to deformation vs the Cl p_x orbital. The $-\Delta x_{PE}$ shows the highest value among the considered electron density deformation, probably due to a sp^2 hybridization on Cl, that guarantees the best overlap with C hybrid orbitals, and implies two lone pairs in sp orbitals, more spreaded out than p orbitals. **3** shows only scant PE values, being equal in the *x* and *y* directions (0.03 Å), since, assuming a sp hybridization in Cl, the two lone pairs occupy p_x and p_y orbitals, almost similarly to the atomic chlorine. In **5**, the C-X bond formation is strongly affected by the imidazole positive charge, thus producing a strong electron density distortion along the C—Cl bond axis (Δz_{PF} percentage variations up to 10%), but not along the direction perpendicular to it ($-\Delta x_{PE}$/$-\Delta y_{PE}$ percentage variation almost null). In the fluorinated systems a similar trend is observed for the PE in the *x* and *y* direction, with a peculiarity regarding the aromatic **4F** system, for which the $-\Delta x_{PE}$ reaches a value of 0.30 Å, well higher than Δz_{PF} value (0.15 Å), thus suggesting a higher density distortion along the *x* vs *z* direction, probably due to the additive effects of both benzene ring aromaticity and fluorine induction.

3.2. σ-hole

The ESP profiles along the *z* axis for all the investigated systems are reported in Fig. 4. The hydrogenated neutral molecules (**1** – **4**) show ESP values increasing for a fixed *z* value passing from a sp^3 to sp^2 and sp hybridization. **5** has a well higher ESP profile, due to the positive charge on the imidazole residue. Interestingly, the ESP profiles show a sign change at long range for the neutral hydrogenated systems, thus suggesting the possibility of a completely different behavior of the hydrogenated vs fluorinated systems in the weak XB interaction. Specifically, we can expect that at long range the interactions involving **1**–**4** molecules, for which the dipole moment is higher with respect to fluorinated **1F** – **4F** substrates, may be steered by the dipole moment, rather than by the σ-hole, that would bring a repulsive contribution.

The fluorinated neutral molecules **1F** – **4F** have bundled ESP profiles, thus suggesting that the fluorination tends to level the hybridization effect. The charged **5F** system has a well higher profile, as already seen for hydrogenated systems. In general, the fluorinated systems have higher ESP values than the hydrogenated ones, except for **3**/**3F**, showing again a negligible effect of the fluorination in this specific case.

The ESP maps of the halogenated systems are reported in Fig. 4b (except for the positively charged **5**/**5F** imidazole systems, showing a completely positive surface in the considered energy range). The chlorine atom in all systems is pointing out of the page and the σ-hole is localized on the top of it. The substitution of the hydrogen with fluorine atoms determines a deepchange on the molecular electrostatic potential map, except for **3**/**3F** systems.

In the hydrogenated neutral molecules, the effect of the hybridization on the computed ESP values also clearly emerges, since the σ-hole magnitude assumes rather different values in **1**–**4** systems. In particular, we computed 0.6 kcal/mol in **1**, 5.6/4.9 kcal/mol in **2**/**4** and even 22.4 kcal/mol in **3**, involving, respectively, a sp^3, sp^2 and sp hybridization type. This trend can be rationalized on the basis of the stronger electron-withdrawing character of the organic moiety bearing a sp vs sp^2 or sp^3 hybridization (see above). The computed values suggest a strong impact

Table 1
PF (Δz_{PF}) and PE (Δx_{PE}, Δy_{PE}) values (Å) for the hydrogenated/fluorinated systems, evaluated at the isodensity reference value of 0.001 e·bohr^{-3}, together with the correspondent percentage variations (%), computed with respect to the isolated Cl coordinate (see text).

Systems	Δz_{PF}	$\frac{\Delta z_{PF}}{z_{Cl(isolated)}} \times 100$	Δx_{PE}	$\frac{\Delta x_{PE}}{x_{Cl(isolated)}} \times 100$	Δy_{PE}	$\frac{\Delta y_{PE}}{y_{Cl(isolated)}} \times 100$
1/1F	0.122/0.143	5.9/7.0	−0.085/−0.053	−4.1/−2.6	−0.090/−0.053	−4.4/−2.6
2/2F	0.122/0.153	5.9/7.4	−0.106/−0.116	−5.6/−8.1	−0.063/−0.047	−3.1/−2.3
3/3F	0.173/0.176	8.4/8.6	−0.029/−0.033	−1.4/−1.6	−0.029/−0.033	−1.4/−1.6
4/4F	0.122/0.153	5.9/7.4	−0.116/−0.296	−8.1/−14.4	−0.063/−0.048	−3.1/−2.3
5/5F	0.207/0.223	10.1/10.8	−0.037/−0.032	−1.8/−1.5	−0.005/0.005	−0.2/0.2

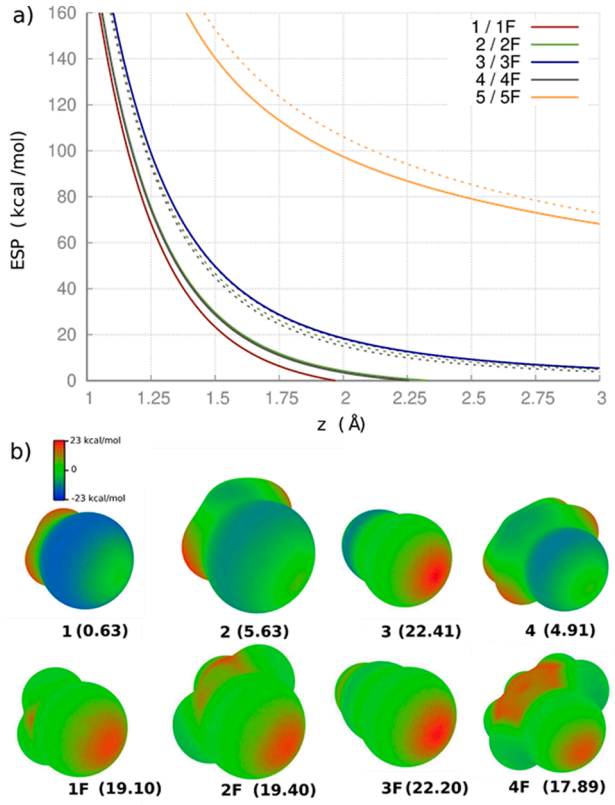

Fig. 4. a) Electrostatic potential energy profile (ESP) along the C-Cl bond axis. Solid /dashed lines refer to hydrogenated/fluorinated systems. b) Molecular electrostatic potential map at 0.001 e·Bohr^{-3} isodensity surface. The σ-hole value is also reported in kcal/mol (see text for details). For the **5**/**5F** systems (not reported in the figure) a σ-hole value of 106.07/116.90 kcal/mol is found.

of the chemical environment on the σ-hole, with the ESP values strongly intensifying passing from hydrogenated to fluorinated neutral systems. Moreover, the σ-hole values of the fluorinated systems present more narrow values with the range of 18–22 kcal/mol, which suggests a damping of the hybridization effect upon the introduction of the more electronegative atoms. As expected from the ESP curves, the σ-hole values are identical in the **3**/**3F** systems. Interestingly, a fairly linear correlation was found between the σ-hole and the PF for the neutral fluorinated moieties, but not for the hydrogenated ones (see Fig. S1 in Supplementary Data), both parameters depending on the C hybridization. The imidazole cation systems **5**/**5F** show well high σ-hole values (106.1/116.9 kcal/mol) because of the positive charge, also concealing the effect of the fluorine atoms replacement.

3.3. Charge transfer (CT) in XB complexes interacting with Cl^- and NH_3

Once the isolated halogenated moieties have been characterized in terms of PF and σ-hole identifiers, it is productive to analyze the CT component occurring upon XB complex formation with suitable electron donating systems, namely Cl^- and NH_3. The CT contribution has been evaluated by means of the CD analysis [20].

The CD curve for the selected adduct **1**-Cl^-, reported in Fig. 5, shows positive Q(e) values everywhere in the molecular region, thus showing that, at each point along the internuclear axis, a net shift of charge from the chloride ion to the halogenated compound has occurred. In particular, the trend of the CD curve describes an electron loss till the chlorine center in the **1** residue, where a rather sharp inversion is attained and the charge starts to re-accumulate rapidly, till about 4 Å from Cl. The isodensity deformation 3D plot, where the charge depletion/accumulation path is signed by green/grey color, confirms a certain amount of

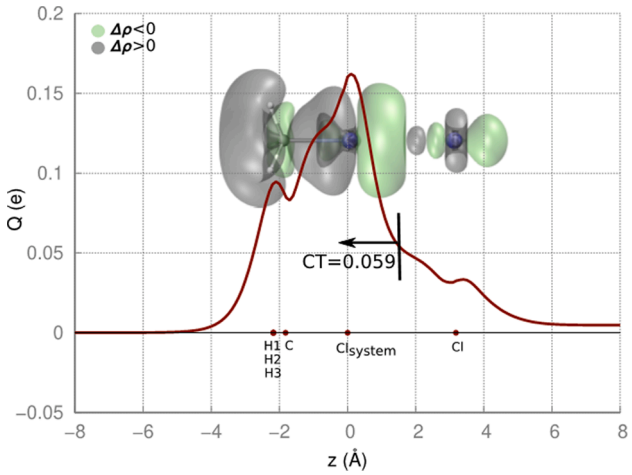

Fig. 5. CD curve (Q vs *z*) of the **1**-Cl^- adduct. The background shows the 3D isodensity plot of the electron density change upon adduct formation ($\Delta\rho = \pm 0.0004$ e·bohr^{-3}, negative/positive values in grey/green). The dots represent the nuclei *z* coordinates; Cl in the halogenated substrate is set on zero and the H nuclei in **1** have fairly the same *z* value. The vertical line identifies a conventional boundary between the CH_3Cl and Cl^- fragments.

charge rearrangement in both partners, with the **1** electron density being strongly polarized by the negative donor.

An analogous trend is observed for the **1**–**5**/**1F**-**5F** complexes with Cl^- and NH_3 Lewis bases (see Figs. 6 and 7), still demonstrating the occurrence of a net shift of charge in the direction from the base ligand to the halogenated substrates. We can therefore conclude that a certain degree of covalency is present in the formed XB adducts. The plotted CD curves indicate that the density electron rearrangements are more pronounced in the complexes with chloride vs ammonia and with fluoride vs hydrogenated partners (since F is a stronger Lewis acid than H). The shape of the CD curves for the **1**–**4**/**1F**-**4F** complexes is very similar, in particular in the region of the ligand electron cloud: at the donor site, the CD curves have a slight negative slope, indicating a reasonable electron depletion, and assume a positive slope in the bond region, suggesting a CT towards the organic moiety. It is eye-catching that the CD curves of the complexes with the imidazole cation moieties (**5**/**5F**) behave differently with respect to those with the neutral organic moieties, because the imidazole positive charge steeply affects the NH_3/Cl^- density. On the halogenated moiety we observed, in the complexes with NH_3, a slight rearrangement, due to the its dipole moment, and, in the complex with Cl^-, a strong polarization, decreasing to zero at the left side, due to the ligand negative charge. A reasonable estimation of the CT occurring upon complex formation can be gathered from the value of *Q* at the IB (see Section 2). For the neutral NH_3 XB complexes the evaluated CT values are very close, (0.015–0.020 electrons, e), in agreement with the above CD curves description, so that a CT trend based on carbon hybridization or inductive effect cannot be easily assessed. Note that almost null CT is computed for **2**-$NH_3$and **4**-NH_3 complexes, that present only a local minimum in the potential energy surface for the XB configuration and result unstable with respect to the isolated fragments (with negative interaction energy, see next section and data in Fig. 1). Not surprisingly, for the charged NH_3 XB complexes higher CT values are computed (0.070/0.124 e for **5**/**5F**). Conversely, the analysis of the CT in the complexes with the anionic Cl^- donor allows to unmask some differences in the interaction with the various halogenated substrates. The CT values are in the range 0.055–0.160 e for the neutral substrates and suggest the lacking of any dependence on the carbon hybridization. As expected, the CT values are higher than that found in the corresponding values for the ammonia complexes, in agreement with the CD curves tendency. The substitution of H with F atoms in **1**, **2**, **5** causes an increase of the CT up to twice, and in **4** even to

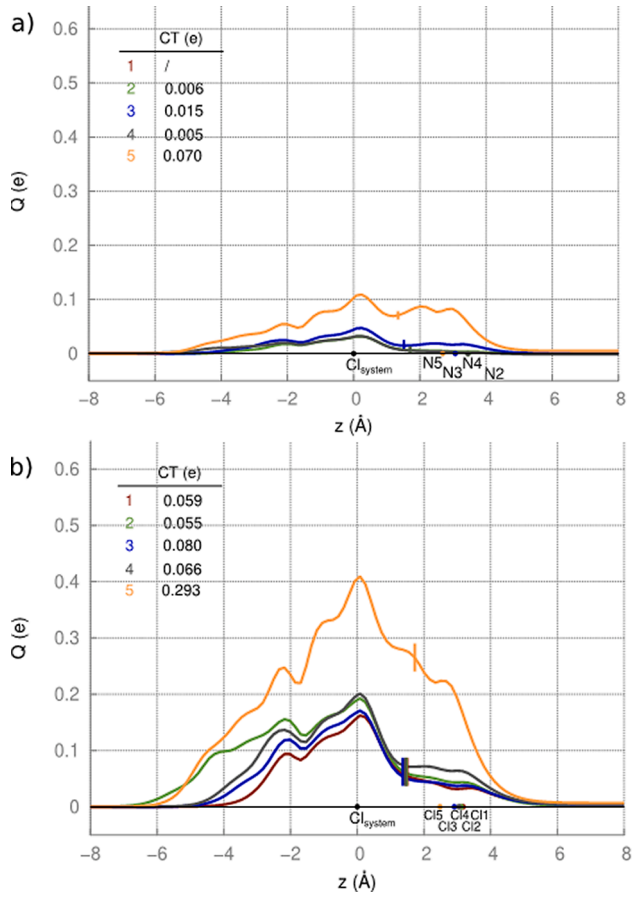

Fig. 6. CD curves (Q vs z) of the adducts with NH_3 (a) and Cl^- (b) with hydrogenated systems **1**–**5**. The vertical solid lines identify a conventional boundary between the interacting partners. The dots on the *z* axis represent the nuclei *z* coordinate for selected atoms, with numbering labels for N and Cl atoms of the Lewis base referring to the involved hydrogenated substrate; the Cl in the X moiety (Cl_{system}) is set on zero. Top left tables in the panels show the computed CT values extracted from the CD curves (see text for details).

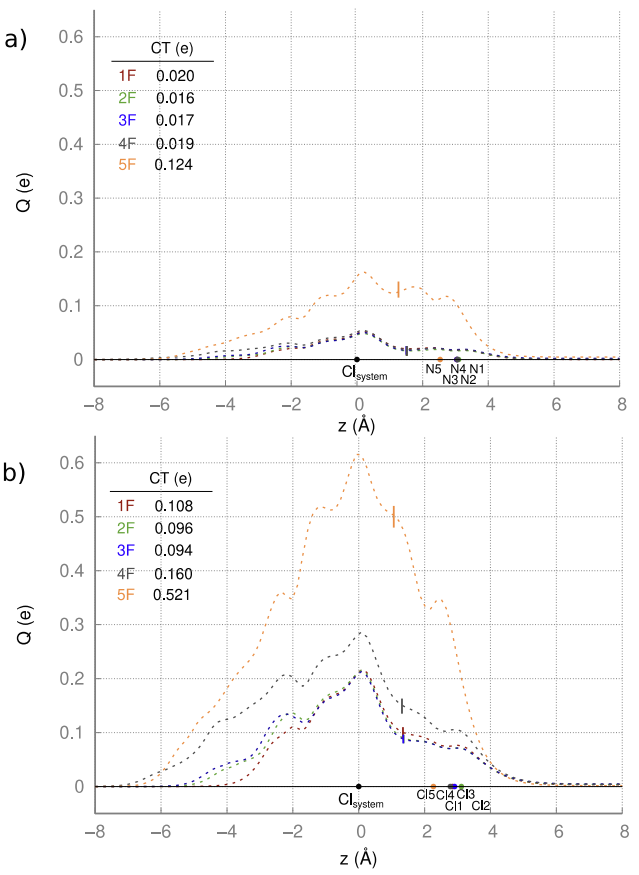

Fig. 7. CD curves (Q vs z) of the adducts with NH_3 (a) and Cl^- (b) with fluorinated systems **1F**-**5F**. The vertical solid lines identify a conventional boundary between the interacting partners. The dots on the *z* axis represent the nuclei *z* coordinate for selected atoms, with numbering labels for N and Cl atoms of the Lewis base referring to the involved fluorinated substrate; the Cl in the X moiety (Cl_{system}) is set on zero. Top left tables in the panels show the computed CT values extracted from the CD curves (see text for details).

three times, while the fluorination in **3** has a negligible effect on the CT, as discussed above. It is important to highlight this result, because it demonstrates that the CT has a stronger dependence on both hybridization and induction effects than other identifiers, such as PF and σ-hole. As discussed above, the fluorine substitution on the benzene ring in **4** system determines an increase of the σ-hole by 13 kcal mol^{-1}, reaching a value of 17.89 kcal mol^{-1}, that, however, is slightly lower than the σ-hole computed for the fluorinated **1F** – **3F** systems (see Fig. 4), while the dipole moment of **4F** (0.3 D) decreases with respect to **4** (1.7 D). Moreover, the PF in **4F** (0.153 Å, see Table 1) is very close to that of the **1F**/**2F**/**3F** neutral systems, but, among the Cl^- halogen complexes, the **4F-Cl**$^-$ adduct transfers the highest charge amount (0.160 e). We also note that the whole CD curve of the **4F-Cl**$^-$ adduct is shifted above the others, suggesting a major rearrangement on the chlorine anion, probably also due to long range effects of the fluorine substituents and of the aromatic ring.

3.4. *Interaction energies in XB complexes interacting with Cl^- and NH_3*

The main bond distances, together with the bond dissociation energies for the XB complexes with NH_3 and Cl^- ligands are reported in Fig. 1 and in Supplementary Data section. The results show that the intermolecular distances are strongly affected by both the C hybridization and F substitution. For those systems (**1-Cl**$^-$, **2-NH$_3$**, **4-NH$_3$**), which are unstable (negative energy interaction in Fig. 1) with respect to the isolated fragments, we report the geometries (and energy) of the local minimum we found in the XB arrangement. A such local minimum is absent in the case of **1-NH$_3$**. For the hydrogenated substrates, the intermolecular distances vary in the order **5** < **3** < **4** ≅ **2** < **1**, for both NH_3 and Cl^- Lewis bases. The bond dissociation energies vary in the reverse order, in fairly agreement with the σ-hole values (see Fig. 4), thus suggesting that this parameter, strongly correlated with the C hybridization (see above), has a key role in these weak bonded adducts. The XB strengths span over a broad range of values. The interaction with NH_3 gives values within 2 kcal mol^{-1} for the neutral substrates and up to 10 kcal mol^{-1} for the imidazole. The replacement of H with electron-withdrawing F atoms strengthens the X-B interaction, with the exception of **3**/**3F** moiety (see above), and significantly levels the influence of the C hybridization, with energy values near 2 kcal mol^{-1} (NH_3 ligand) and between 12 and 14 kcal mol^{-1} (Cl^- ligand) for the neutral substrates. As expected, the imidazole cation **5F** returns higher values, 14.69 and 136.11 kcal mol^{-1} respectively with the NH_3 and Cl^- bases. We can conclude that, independently on the ligand partner, the inductive effect of the fluorine atoms determines a smoothening of the bond dissociation energies. The same levelling effect was discussed for the σ-hole (see above). Indeed, reporting a plot of the dissociation energy vs the σ-hole (see Figure S2a in Supplementary Data), a good linear correlation was found only for neutral hydrogenated systems with both NH_3 and Cl^- bases, but not for the fluorinated ones. Vice versa, a rough linear correlation was found for neutral hydrogenated systems with both NH_3 and Cl^- bases, but not for the fluorinated ones. A rough linear

correlation was also found between the dissociation energies and the amount of CT for the complexes of neutral fluorinated moieties with the Cl^- base (Figure S2b in Supplementary Data), even if, clearly, other contributions besides the CT component concur to the XB interaction. However, the same correlation with the systems with NH_3 is completely lost.

4. Conclusions

A series of systems bearing carbon-chlorine (C—Cl) bond and their complexes with two representative donors have been examined by quantum-chemistry DFT calculations to gain a deeper insight into the parameters affecting the HB interaction. In particular, we considered the effect of the C hybridization and induction through H/F substitution on the PF, σ-hole and CT in the XB complexes. Among the neutral substrates, the PF is computed higher in sp-hybridized carbon-bound X systems, while the sp^2 and sp^3 ones show fairly the same (lower) PF value, thus suggesting a certain transferability of this identifier. The fluorine substitution determines an increase by 0.02–0.03 Å in the PF, except for ethylene, lacking of F atoms directly bounded to halogenated C atom. The PF amount plays a key role in the description of the position and strength of the repulsive wall in the XB interaction, so that it strongly affects the XB intermolecular distances. The σ-hole is computed to increase in the order $sp^3 < sp^2 < sp$ in both the neutral hydrogenated and fluorinated substrates, even if the F substitution causes a strong leveling, thus suggesting that in fluorinated systems the σ-hole is a transferable identifier. The CD analysis proves that the CT component is not strictly dependent on the C hybridization and is increased upon F substitution. The positively charged imidazole cation substrate shows PF, σ-hole and CT well higher than the neutral systems, thus confirming the importance of the electrostatic contribution to the XB interaction. The findings and the systematic approach we employed here to investigate how typical descriptors for XB depend on the chemical environment may contribute to a more rational design of force-fields, aimed at the modelling of the XB interaction in more complex systems with a high level of accuracy.

CRediT authorship contribution statement

Francesca Nunzi: Writing - review & editing, Visualization, Validation, Formal analysis, Funding acquisition. **Diego Cesario:** Investigation, Data curation, Writing - original draft. **Francesco Tarantelli:** Project administration. **Leonardo Belpassi:** Supervision, Writing - review & editing.

Declaration of Competing Interest

The authors declare that they have no known competing financial interests or personal relationships that could have appeared to influence the work reported in this paper.

Acknowledgements

D. C., F. N. and F. T. acknowledge support from the Ministero dell'Università e della Ricerca (MUR) and the University of Perugia through the program "Dipartimenti di Eccellenza 2018–2022" (grant AMIS) and the University of Perugia for funding through the "Fondo Ricerca di Base 2017" programme.

Appendix A. Supplementary material

Supplementary data to this article can be found online. Geometrical parameters for the optimized structures; correlation plots of bond dissociation energies and σ-hole, CT and PF.

Supplementary data to this article can be found online at https://doi.org/10.1016/j.cplett.2021.138522.

References

[1] G.R. Desiraju, P.S. Ho, L. Kloo, A.C. Legon, R. Marquardt, P. Metrangolo, P. Politzer, G. Resnati, K. Rissanen, Definition of the halogen bond (IUPAC Recommendations 2013), Pure Appl. Chem. 85 (8) (2013) 1711–1713.
[2] J. Thirman, E. Engelage, S.M. Huber, M. Head-Gordon, Characterizing the interplay of Pauli repulsion, electrostatics, dispersion and charge transfer in halogen bonding with energy decomposition analysis, Phys. Chem. Chem. Phys. 20 (2) (2018) 905–915.
[3] A.J. Stone, Are halogen bonded structures electrostatically driven? J. Am. Chem. Soc. 135 (18) (2013) 7005–7009.
[4] F. Nunzi, G. Pannacci, F. Tarantelli, L. Belpassi, D. Cappelletti, S. Falcinelli, F. Pirani, Leading interaction components in the structure and reactivity of noble gases compounds, Molecules 25 (10) (2020).
[5] F. Pirani, D. Cappelletti, S. Falcinelli, D. Cesario, F. Nunzi, L. Belpassi, F. Tarantelli, Selective emergence of halogen bond in ground and excited states of noble-gas—chlorine systems, Angew. Chem. Int. Ed. 58 (2019) 4195–4199.
[6] F. Nunzi, D. Cesario, L. Belpassi, F. Tarantelli, L.F. Roncaratti, S. Falcinelli, D. Cappelletti, F. Pirani, Insight into the halogen-bond nature of Noble gas-chlorine systems by molecular beam scattering experiments, ab initio calculations and charge displacement analysis, Phys. Chem. Chem. Phys. 21 (14) (2019) 7330–7340.
[7] F. Nunzi, B. Di Erasmo, F. Tarantelli, D. Cappelletti, F. Pirani, The halogen-bond nature in noble gas-dihalogen complexes from scattering experiments and ab initio calculations, Molecules 24 (23) (2019) 4274.
[8] M. De Santis, F. Nunzi, D. Cesario, L. Belpassi, F. Tarantelli, D. Cappelletti, F. Pirani, Cooperative role of halogen and hydrogen bonding in the stabilization of water adducts with apolar molecules, New J. Chem. 42 (13) (2018) 10603–10614.
[9] J.W. Zou, Y.J. Jiang, M. Guo, G.X. Hu, B. Zhang, H.C. Liu, Q.S. Yu, Ab initio study of the complexes of halogen-containing molecules RX (X = Cl, Br, and I) and NH_3: towards understanding the nature of halogen bonding and the electron-accepting propensities of covalently bonded halogen atoms, Chem. Eur. J. 11 (2) (2005) 740–751.
[10] S. Scheiner, F-halogen bond: conditions for its existence, J. Phys. Chem. A 124 (36) (2020) 7290–7299.
[11] G. Cavallo, P. Metrangolo, R. Milani, T. Pilati, A. Priimagi, G. Resnati, G. Terraneo, The halogen bond, Chem. Rev. 116 (4) (2016) 2478–2601.
[12] T. Clark, M. Hennemann, J.S. Murray, P. Politzer, Halogen bonding: the σ-hole, J. Mol. Model. 13 (2) (2007) 291–296.
[13] P. Politzer, J.S. Murray, T. Clark, Halogen bonding and other ◆-hole interactions: a perspective, Phys. Chem. Chem. Phys. 15 (27) (2013) 11178–11189.
[14] M.H. Kolář, P. Hobza, Computer modeling of halogen bonds and other σ-Hole interactions, Chem. Rev. 116 (9) (2016) 5155–5187.
[15] R. Sedlak, M.H. Kolar, P. Hobza, Polar flattening and the strength of halogen bonding, J. Chem. Theory Comput. 11 (10) (2015) 4727–4732.
[16] E. Rossi, M. De Santis, D. Sorbelli, L. Storchi, L. Belpassi, P. Belanzoni, Spin-orbit coupling is the key to unraveling intriguing features of the halogen bond involving astatine, Phys. Chem. Chem. Phys. 22 (4) (2020) 1897–1910.
[17] J. Rezac, A. de la Lande, On the role of charge transfer in halogen bonding, Phys. Chem. Chem. Phys. 19 (1) (2017) 791–803.
[18] V. Oliveira, E. Kraka, D. Cremer, The intrinsic strength of the halogen bond: electrostatic and covalent contributions described by coupled cluster theory, Phys. Chem. Chem. Phys. 18 (48) (2016) 33031–33046.
[19] S.M. Huber, E. Jimenez-Izal, J.M. Ugalde, I. Infante, Unexpected trends in halogen-bond based noncovalent adducts, Chem. Comm. 48 (62) (2012) 7708–7710.
[20] L. Belpassi, I. Infante, F. Tarantelli, L. Visscher, The chemical bond between Au(I) and the noble gases. Comparative study of NgAuF and $NgAu^+$ (Ng = Ar, Kr, Xe) by density functional and coupled cluster methods, J. Am. Chem. Soc. 130 (3) (2008) 1048–1060.
[21] A.D. Becke, Density-functional exchange-energy approximation with correct asymptotic-behavior, Phys. Rev. A 38 (6) (1988) 3098–3100.
[22] J.P. Perdew, Density-functional approximation for the correlation-energy of the inhomogeneous electron-gas, Phys. Rev. B 33 (12) (1986) 8822–8824.
[23] M.J. Frisch, G.W. Trucks, H.B. Schlegel, G.E. Scuseria, M.A. Robb, J.R. Cheeseman, G. Scalmani, V. Barone, B. Mennucci, G.A. Petersson, H. Nakatsuji, M. Caricato, X. Li, H.P. Hratchian, A.F. Izmaylov, J. Bloino, G. Zheng, J.L. Sonnenberg, M. Hada, M. Ehara, K. Toyota, R. Fukuda, J. Hasegawa, M. Ishida, T. Nakajima, Y. Honda, O. Kitao, H. Nakai, T. Vreven, J.A. Montgomery, J.E.P. Jr., F. Ogliaro, M. Bearpark, J. J. Heyd, E. Brothers, K.N. Kudin, V.N. Staroverov, R. Kobayashi, J. Normand, K. Raghavachari, A. Rendell, J.C. Burant, S.S. Iyengar, J. Tomasi, M. Cossi, N. Rega, J. M. Millam, M. Klene, J.E. Knox, J.B. Cross, V. Bakken, C. Adamo, J. Jaramillo, R. Gomperts, R.E. Stratmann, O. Yazyev, A.J. Austin, R. Cammi, C. Pomelli, J.W. Ochterski, R.L. Martin, K. Morokuma, V.G. Zakrzewski, G.A. Voth, P. Salvador, J.J. Dannenberg, S. Dapprich, A.D. Daniels, Ö. Farkas, J.B. Foresman, J.V. Ortiz, J. Cioslowski, D.J. Fox, Gaussian09. Revision D, Gaussian, Inc., Wallingford CT, 2009.
[24] T.H. Dunning, Gaussian-basis sets for use in correlated molecular calculations. 1. The atoms boron through neon and hydrogen, J. Chem. Phys. 90 (2) (1989) 1007–1023.
[25] A.D. Becke, Density-functional thermochemistry 3. The role of exaxct exchange, J. Chem. Phys. 98 (7) (1993) 5648–5652.
[26] P.J. Stephens, F.J. Devlin, C.F. Chabalowski, M.J. Frisch, Ab-initio calculation of vibrational absorption and circular-dichroism spectra using density-functional force-fields, J. Phys. Chem. 98 (45) (1994) 11623–11627.

[27] C. Adamo, V. Barone, Toward reliable density functional methods without adjustable parameters: the PBE0 model, J. Chem. Phys. 110 (13) (1999) 6158–6170.
[28] T. Yanai, D.P. Tew, N.C. Handy, A new hybrid exchange-correlation functional using the Coulomb-Attenuating Method (CAM-B3LYP), Chem. Phys. Lett. 393 (1–3) (2004) 51–57.
[29] K. Raghavachari, G.W. Trucks, J.A. Pople, M. Headgordon, A 5th-order perturbation comparison of electron correlation theories, Chem. Phys. Lett. 157 (6) (1989) 479–483.
[30] H.J. Werner, P.J. Knowles, G. Knizia, F.R. Manby, M. Schutz, Molpro: A general-purpose quantum chemistry program package, Wiley Interdiscip. Rev. Comput. Mol. Sci. 2 (2) (2012) 242–253.
[31] R.F.W. Bader, M.T. Carroll, J.R. Cheeseman, C. Chang, Properties of atoms in molecules: atomic volumes, J. Am. Chem. Soc. 109 (26) (1987) 7968–7979.
[32] D. Cesario, M. Fortino, T. Marino, F. Nunzi, N. Russo, E. Sicilia, The role of the halogen bond in iodothyronine deiodinase: dependence on chalcogen substitution in naphthyl-based mimetics, J. Comput. Chem. 40 (8) (2019) 944–951.
[33] S. Borocci, F. Grandinetti, N. Sanna, P. Antoniotti, F. Nunzi, Noncovalent complexes of the Noble-Gas Atoms: analyzing the transition from physical to chemical interactions, J. Comput. Chem. 40 (26) (2019) 2318–2328.
[34] F. Nunzi, D. Cesario, F. Pirani, L. Belpassi, F. Tarantelli, Modelling Charge Transfer in Weak Chemical Bonds: Insights from the Chemistry of Helium, ChemPhysChem 19 (12) (2018) 1476–1485.